

Supporting Information

Title

Correlation between oxygen evolution reaction activity and surface compositional evolution in epitaxial $\text{La}_{0.5}\text{Sr}_{0.5}\text{Ni}_{1-x}\text{Fe}_x\text{O}_{3-\delta}$ thin films

Author Names and affiliations

Prajwal Adiga¹, Le Wang^{2,*}, Cindy Wong¹, Bethany E. Matthews³, Mark E. Bowden⁴, Steven R. Spurgeon^{3,5}, George E. Sterbinsky⁶, Monika Blum,⁷ Min-Ju Choi², Jinhui Tao², Tiffany C. Kaspar², Scott A. Chambers², Kelsey A. Stoerzinger^{1,2,*}, Yingge Du²

¹ School of Chemical, Biological and Environmental Engineering, Oregon State University, Corvallis, Oregon, 97331, USA

² Physical and Computational Sciences Directorate, Pacific Northwest National Laboratory, Richland, Washington 99354, USA

³ Energy and Environment Directorate, Pacific Northwest National Laboratory, Richland, Washington 99352, USA

⁴ Environmental Molecular Sciences Laboratory, Pacific Northwest National Laboratory, Richland, Washington 99352, USA

⁵ Department of Physics, University of Washington, Seattle, Washington 98195, USA

⁶ Advanced Photon Source, Argonne National Laboratory, Lemont, Illinois 60439, USA

⁷ Advanced Light Source, Lawrence Berkeley National Laboratory, Berkeley, California 94720 USA

Corresponding author

* Email address: le.wang@pnnl.gov; kelsey.stoerzinger@oregonstate.edu

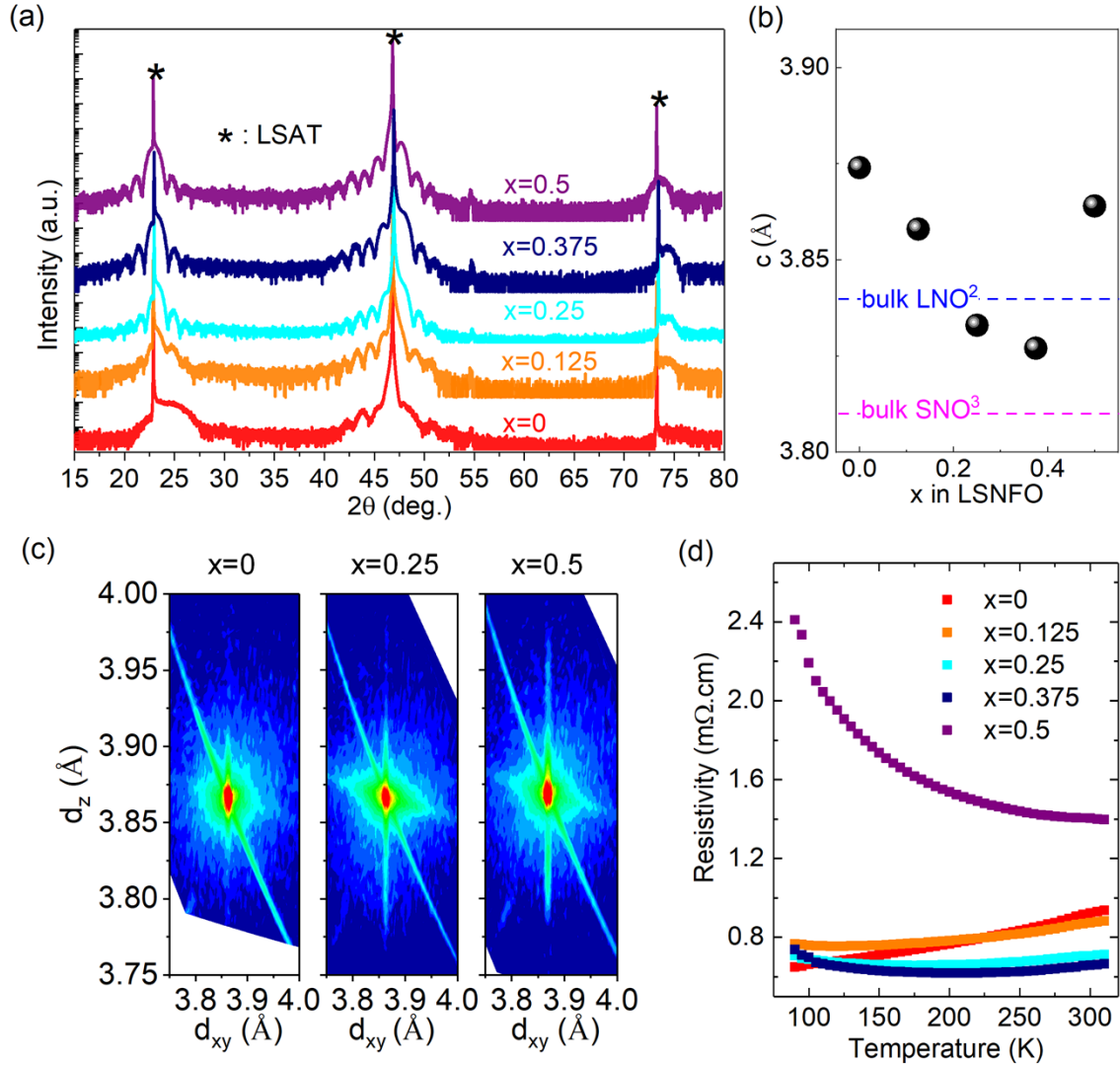


Fig. S1: (a) Extended XRD $0-2\theta$ scans for $\text{La}_{0.5}\text{Sr}_{0.5}\text{Ni}_{1-x}\text{Fe}_x\text{O}_{3-\delta}$ (LSNFO) solid solution epitaxial films grown on LSAT. The peak near 55° in the XRD scans originates from our XRD setup.¹ (b) Reciprocal space maps for LSNFO films confirm structural coherence. (c) Out-of-plane lattice parameter (c) as a function of Fe content (x) in LSNFO. The blue and purple dashed lines denote the pseudo-cubic lattice constants for bulk LNO and bulk SrNiO_3 ,^{2,3} based on which the pseudo-cubic lattice constant of bulk $\text{La}_{0.5}\text{Sr}_{0.5}\text{NiO}_3$ should be $\sim 3.825 \text{ \AA}$, which is smaller than that (3.868 \AA) of the LSAT substrate. Hence, c for the $x = 0$ film is expected to be smaller than the bulk value (3.825 \AA). With Fe doping, c for $x > 0$ films is expected to be larger than that of the $x = 0$ film due to the larger pseudo-cubic lattice constant ($\sim 3.883 \text{ \AA}$)⁴ of bulk $\text{La}_{0.5}\text{Sr}_{0.5}\text{FeO}_3$ compared to bulk $\text{La}_{0.5}\text{Sr}_{0.5}\text{NiO}_3$. However, experimentally we observed larger value c ($\sim 3.875 \text{ \AA}$) for the $x = 0$ film and the decrease of c with increasing x from 0.125 to 0.375, suggesting that these solid solution samples may contain non-negligible amounts of oxygen vacancies. (d) Resistivity versus temperature curves for LSNFO films on heating.

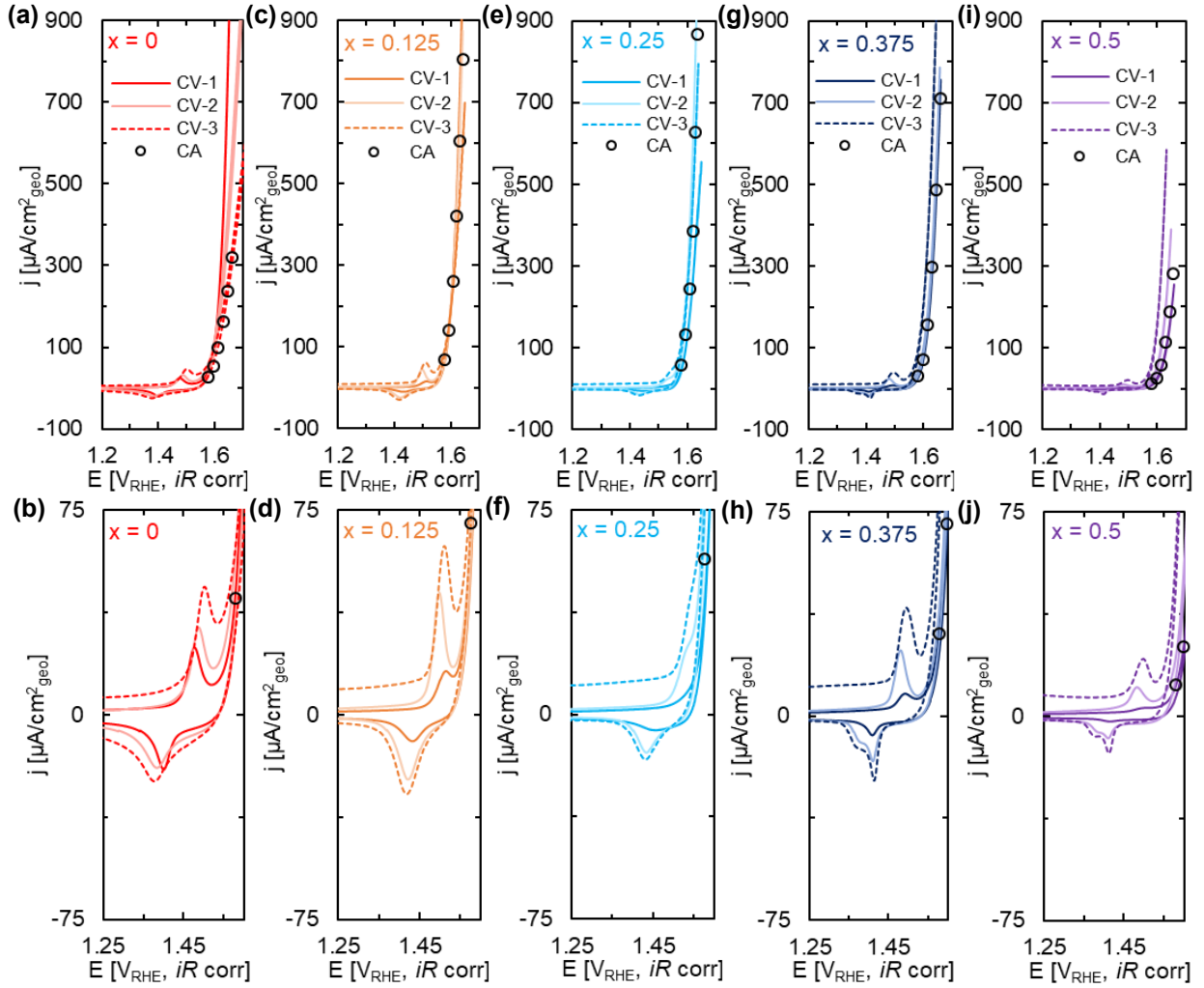


Fig. S2: (a-e) Cyclic voltammetry (CV) and chronoamperometric (CA) measurements for LSNFO films show time-dependent activity changes. The redox peaks for $x \geq 0.375$ show secondary Ni reduction peak indicative of a secondary Ni phase.

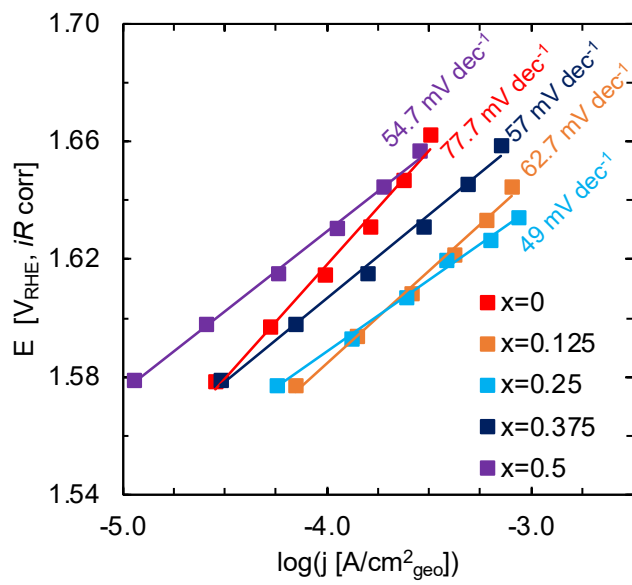


Fig. S3: Tafel slopes for LSNFO.

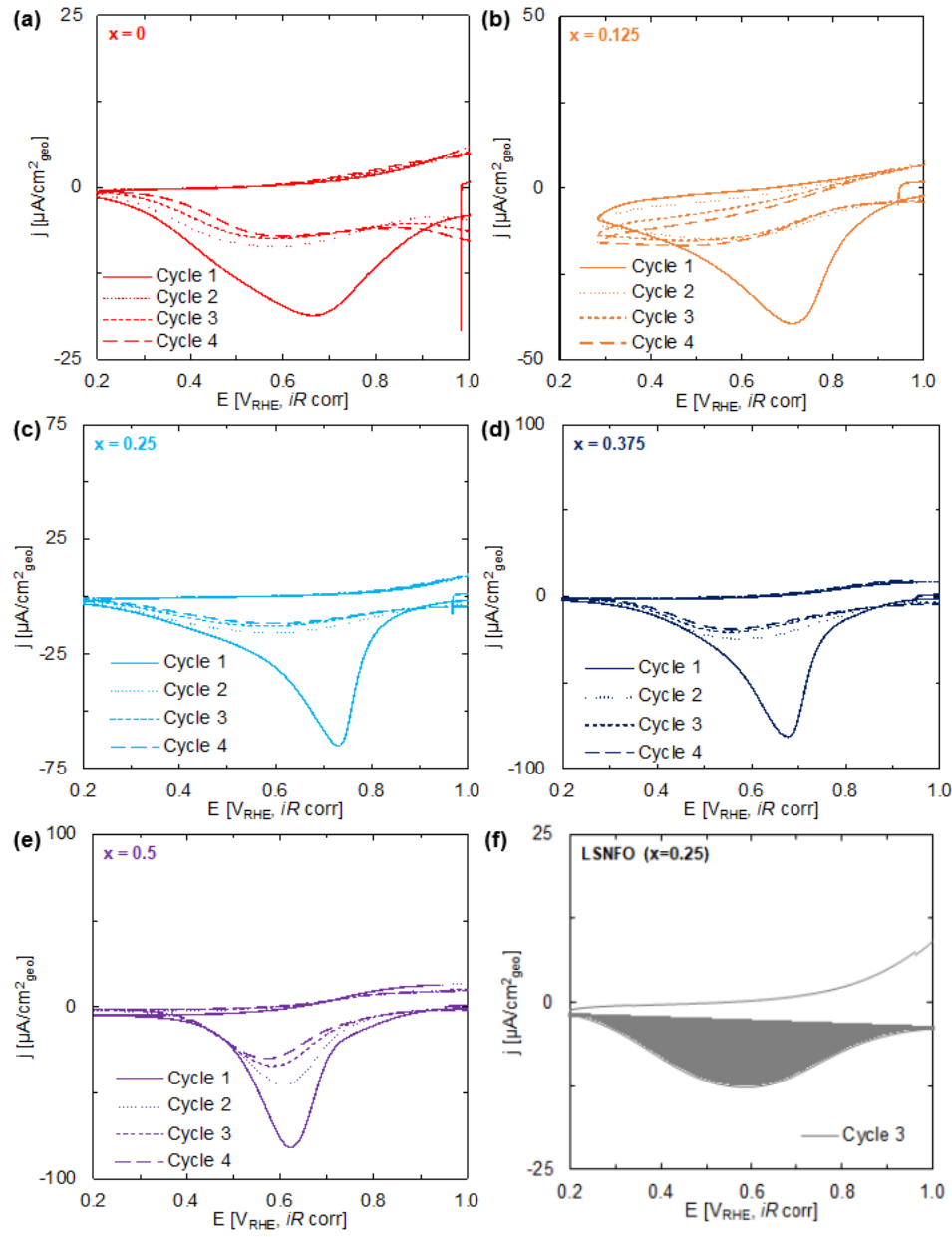


Fig. S4: (a-e) Fe reduction region of CV-3 for compositions $x = 0 - 0.5$, and decreasing magnitude of charge associated with Fe reduction with cycle number. (f) Example of the integrated reduction peak, multiplied by the sweep rate (10 mV/s) to estimate the reduction charge for Fe.

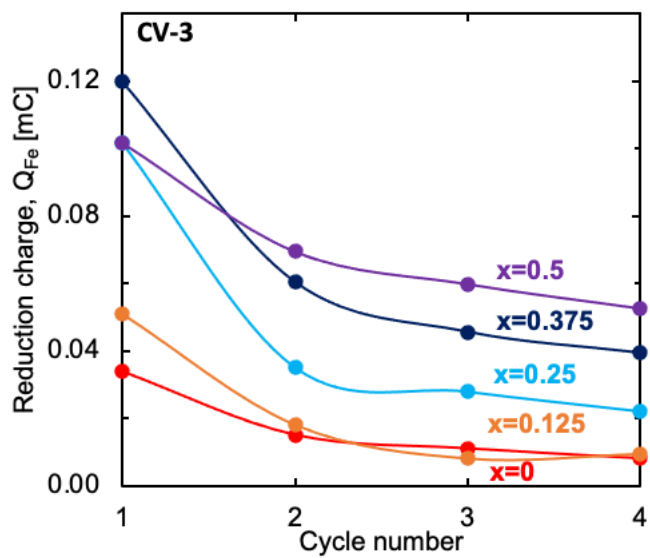


Fig S5: Dynamic changes in the Fe reduction charge indicates dynamic nature of Fe adsorption from trace Fe species in the solution.⁵ In contrast, Ni reduction charge generally increased with cycling during CV-3 (inset of Figure 3b).

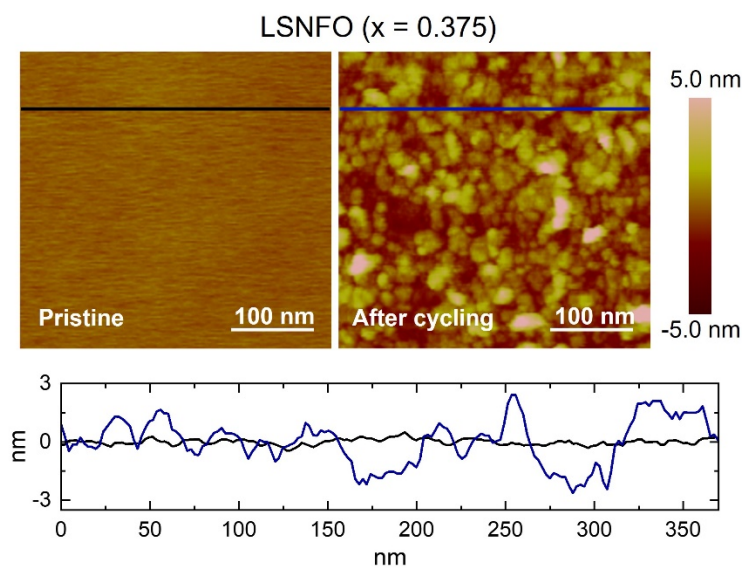


Fig. S6: Atomic force microscopy (AFM) images on selected LSNFO films show larger surface roughness after cycling.

Theoretical calculation for estimating surface Ni (Sample calculation for x = 0.375)

Assume idealized cubic cell structure for the perovskite oxide:

$$\text{Unit cell area, } A_{u.c.} = c^2 = (3.822 \times 10^{-10})^2 = 1.48 \times 10^{-19} m^2$$

where, c = Lattice parameter (in Å)

$$\text{Geometric area of the electrode, } A_{geo} = \frac{\pi}{4} d^2 = \frac{\pi}{4} \left(\frac{1}{8} \times 0.0254\right)^2 = 7.9173 \times 10^{-6} m^2$$

$$\text{Number of unit cells, } n_{u.c.} = \frac{A_{geo}}{A_{u.c.}} = \frac{7.9173 \times 10^{-6}}{1.48 \times 10^{-19}} = 5.42 \times 10^{13}$$

With one B-site atom per perovskite unit cell,

$$\text{Total Ni atoms, } N_{Ni} = n_{u.c.} x (1 - 0.375) = 5.42 \times 10^{13} \times (1 - 0.375) = 3.39 \times 10^{13} \text{ atoms}$$

$$\text{Estimated Ni atoms per m}^2, \frac{N_{Ni}}{A_{geo}} = \frac{3.39 \times 10^{13}}{7.9173 \times 10^{-6}} = 4.28 \times 10^{18} \frac{\text{atoms}}{m^2}$$

$$\text{Estimated Ni atoms per nm}^2, \frac{4.28 \times 10^{18} \text{ atoms}}{(10^9)^2 \text{ nm}^2} = 4.28 \frac{\text{atoms}}{\text{nm}^2}$$

Reference

1. L. Wang, Z. Yang, X. Yin, S. D. Taylor, X. He, C. S. Tang, M. E. Bowden, J. Zhao, J. Wang, J. Liu, D. E. Pereira, L. Wangoh, A. T. S. Wee, H. Zhou, S. A. Chambers and Y. Du, *Science Advances*, 2021, **7**, eabe2866.
2. A. S. Disa, D. P. Kumah, J. H. Ngai, E. D. Specht, D. A. Arena, F. J. Walker and C. H. Ahn, *APL Materials*, 2013, **1**, 032110.
3. L. Wang, Z. Yang, M. E. Bowden, J. W. Freeland, P. V. Sushko, S. R. Spurgeon, B. Matthews, W. S. Samarakoon, H. Zhou, Z. Feng, M. H. Engelhard, Y. Du and S. A. Chambers, *Advanced Materials*, 2020, **32**, 2005003.
4. X. N. Ying and L. Zhang, *Solid State Communications*, 2012, **152**, 1252-1255.
5. P. P. Lopes, D. Y. Chung, X. Rui, H. Zheng, H. He, P. Farinazzo Bergamo Dias Martins, D. Strmcnik, V. R. Stamenkovic, P. Zapol, J. F. Mitchell, R. F. Klie and N. M. Markovic, *Journal of the American Chemical Society*, 2021, **143**, 2741-2750.